frontiers | Frontiers in Earth Science

TYPE Original Research
PUBLISHED 16 January 2023
DOI 10.3389/feart.2022.994850

Check for updates

OPEN ACCESS

EDITED BY
Hongfeng Yang,
The Chinese University of Hong Kong, China

REVIEWED BY
Andrea Llenos,
U.S. Geological Survey, United States
Rita Di Giovambattista,
Istituto Nazionale di Geofisica e Vulcanologia (INGV), Italy

*CORRESPONDENCE
Fengling Yin,
yinfengling@cea-igp.ac.cn
Changsheng Jiang,
jiangcs@cea-igp.ac.cn

SPECIALTY SECTION
This article was submitted to Solid Earth Geophysics,
a section of the journal
Frontiers in Earth Science

RECEIVED 15 July 2022
ACCEPTED 15 November 2022
PUBLISHED 16 January 2023

CITATION
Bi J, Yin F, Jiang C, Yin X, Ma Y and Song C (2023), Strong aftershocks traffic light system: A case study of the 8 January 2022 M_S6.9 Menyuan earthquake, Qinghai Province, China. *Front. Earth Sci.* 10:994850. doi: 10.3389/feart.2022.994850

COPYRIGHT
© 2023 Bi, Yin, Jiang, Yin, Ma and Song. This is an open-access article distributed under the terms of the Creative Commons Attribution License (CC BY). The use, distribution or reproduction in other forums is permitted, provided the original author(s) and the copyright owner(s) are credited and that the original publication in this journal is cited, in accordance with accepted academic practice. No use, distribution or reproduction is permitted which does not comply with these terms.

Strong aftershocks traffic light system: A case study of the 8 January 2022 M_S6.9 Menyuan earthquake, Qinghai Province, China

Jinmeng Bi[1,2], Fengling Yin[1]*, Changsheng Jiang[1]*, Xinxin Yin[1,3], Yong Ma[2] and Cheng Song[2]

[1]Institute of Geophysics, China Earthquake Administration, Beijing, China, [2]Tianjin Earthquake Agency, Tianjin, China, [3]Gansu Earthquake Agency, Lanzhou, China

Strong aftershocks, especially the disaster-causing M≥5.0 kind, are a key concern for mitigation of seismic risks because they often lead to superimposed earthquake damage. However, the real-time forecasting results of the traditional probability prediction models based on statistics are usually far from accurate and therefore unsatisfactory. Borrowing an idea from the foreshock traffic light system (FTLS), which is based on observations of decreasing b-values or increasing differential stress just before a strong aftershock, we constructed a strong aftershock traffic light system (SATLS) that uses data-driven technology to improve the reliability of time sequence b-value calculations, and analyzed the b-value variations of strong aftershocks in the China continent. We applied this system to the M_S6.9 Menyuan earthquake occurred on 8 January 2022. The earthquake occurrence rates before the largest aftershock (M_S5.2) forecast by the Omi-R-J model were too low, although the model could accurately forecast aftershock rates for each magnitude interval in most time-periods. However, reliable b-values can be calculated using the time-sequence b-value data-driven (TbDD) method, and the results showed that the b-values continued declining from 1.3 days before the M_S5.2 aftershock and gradually recovered afterward. This would suggest that the stress evolution in the focal area can provide data for deciding when to post risk alerts of strong aftershocks. In the process of building the SATLS, we studied thirty-four M≥6.0 intraplate earthquake sequences in the China continent and concluded that the differences between the b-values of the aftershock sequences and of the background events, $\triangle b = b_{after} - b_{bg} = \pm 0.1$, could be used as thresholds to determine whether M≥5.0 aftershocks would occur. The $\triangle b$ value obtained using the events before the M_S5.2 aftershock of the M_S6.9 Menyuan sequence was about -0.04, which would have caused the SATLS to declare a yellow alert, but there would have been some gap expected before a red alert was triggered by the b-value difference derived from the events associated with this strong aftershock. To accurately forecast a strong aftershock of M≥5.0, a deeper understanding of the true b-value and a detailed description of the stress evolution state in the source area is necessary.

KEYWORDS

Ogata–Katsura 1993 model, Omi–Reasenberg–Jones model, time-sequence *b*-value data-driven (TbDD) method, aftershock forecasting, traffic light system

Introduction

The disastrous effects of superimposed strong aftershocks on buildings and structures have aggravated casualties and property losses, such as occurred in the *M*7.1 Luanxian strong aftershock and the *M*6.9 Ninghe strong aftershock after the 1976 *M*7.8 Tangshan earthquake (Lv et al., 2007) and the strong *M*6.3 aftershock after the 2010 *M*7.1 earthquake in New Zealand (Zhang et al., 2011). Accurate and reliable forecasting of strong aftershocks is of great importance to post-earthquake emergency evacuation, secondary disaster disposal, and decision-making for restoration and reconstruction (Woessner et al., 2011; Nanjo et al., 2012; Ogata et al., 2013). Traditional strong aftershock forecasting, which is realized mainly by short-term probability forecasting models (Jiang et al., 2018; Bi et al., 2020; Bi and Jiang, 2020) such as the Reasenberg–Jones (R-J) model (Reasenberg and Jones, 1989), the epidemic-type aftershock sequence (ETAS) model (Ogata, 1989), and the Omi-R-J model (Omi et al., 2013, 2015, 2016), still faces great challenges in real-time functionality and accuracy (Lippiello et al., 2017). For example, the Japan Meteorological Agency (JMA) announced a low-probability forecast of $M \geq 5.5$ aftershocks for the 2005 *M*7.0 earthquake off the coast of western Fukuoka Prefecture, Kyushu District, Japan; but, in fact, the earthquake was followed by the largest aftershock of *M*5.8 (Ogata, 2006). In addition, using only the ETAS model to predict the frequency of strong aftershocks in Japan and Southern California (Grimm et al., 2021) and the largest expected aftershock of the 2019 Ridgecrest earthquake sequence in the United States (Shcherbakov, 2021) revealed the model's obvious shortcomings.

In recent years, a new route for the development of strong aftershock forecasting technology has employed the concept of graded risk assessment to improve the operability of forecasting based on abnormal aftershock activity (Matsu'ura, 1986; Ogata, 2001). Gulia and Wiemer (2019) proposed the foreshock traffic light system (FTLS), which uses *b*-values that are sensitive to stress changes, and achieved good results in earthquake cases studies. The theoretical basis of FTLS posits that the *b*-value in relation to G-R can be used as an indirect description of underground differential stress (Gutenberg and Richter, 1944; Scholz, 1968; Scholz, 2015), and that the change in *b*-value is related to the state of underground stress load (Chan and Chandler, 2001; Nandan et al., 2017; Si and Jiang, 2019); some earthquake cases studies showed that the *b*-value can increase by 20% after the main shock and decrease by 10% or more before the strong aftershock (Gulia et al., 2018; Gulia and Wiemer, 2019). Nanjo *et al.* (2022) further improved FTLS by combining local aseismic slips with stress changes. In addition, the idea of a risk classification traffic light system was also widely applied in research of induced earthquake risk control (Jiang et al., 2021b), aftershock hazard analysis (Gulia et al., 2020), and risk assessment of cumulative structural damage caused by aftershocks (Trevlopoulos et al., 2020). However, there is still room for further development in the technical route of strong aftershock forecasting. This can be accomplished through improvements in the risk classification method by an empirical understanding that the *b*-value change of aftershocks compared to that before the earthquake is universal in different tectonic regions and an increased awareness of the influence of subjectivity in the calculation of time series *b*-values (Jiang et al., 2021a; Jiang et al., 2021).

On 8 January 2022, an M_S6.9 earthquake struck Menyuan County, Qinghai Province, northwestern China, and ruptured the Tuolaishan fault (TLSF) and the Lenglongling fault (LLLF) for about 415 km. It affected nearly 6,000 people, damaged more than 4,000 homes and buildings, and caused a large number of secondary disasters such as local slope collapse, rolling stones, cracking of frozen soil, and arch deformation of ice surfaces (https://m.gmw.cn/baijia/2022-01/20/35460649.html). Two strong aftershocks of M_S5.1 and M_S5.2 occurred on January 8 and January 12, respectively, and the latter caused the aftershock area to extend more than 10 km toward the southeast, which was close to the aftershock area of the 2016 M_S6.4 Menyuan earthquake. This phenomenon brought widespread concerns about the strong aftershock risk of the 2022 M_S6.9 Menyuan earthquake. To investigate this risk, we first carried out quantitative aftershock probability forecasting and analyzed the forecasting effectiveness. Second, based on cases studies of the time evolution of *b*-values of intraplate earthquake sequences in the China continent and the occurrence regularity of strong aftershocks, we constructed a strong aftershock traffic light system (SATLS), which is more universal than the FTLS, to qualitatively evaluate the risk of strong aftershocks after the 2022 M_S6.9 Menyuan earthquake. This study provides a scientific basis for improving the forecasting of strong aftershocks following similar complex earthquake sequences.

Quantitative forecasting using the Omi-R-J model

We used the Omi-R-J model (Omi et al., 2013) to conduct aftershock probability forecasting for the M_S6.9 Menyuan earthquake sequence and evaluated the performance of this forecasting method. The Omi-R-J model, which combines the traditional R-J model (Reasenberg and Jones, 1989) with the OK1993 model (Ogata and Katsura, 1993) describing the

magnitude–frequency relationship in the form of a continuous function, can make full use of a large number of small earthquakes below the completeness magnitude in the early stages of an earthquake sequence and produce relatively reliable and stable results in terms of parameter fitting to the model and forecasting of the aftershock occurrence rate. Under the conditions of a non-cumulative magnitude–frequency distribution, the OK1993 model is expressed as:

$$\lambda(M) = \lambda_0(M)q(M), \tag{1}$$

$$\lambda_0\left(M|\beta\right) = \exp\left(-\beta M\right), \tag{2}$$

where M is magnitude and $\beta = b\ln 10$. $q(M)$ is a probability function, which describes the detection-rate of earthquakes and ranges [0, 1]. It is expressed in the form of a cumulative normal distribution:

$$q\left(M|\mu,\sigma\right) = \frac{1}{\sqrt{2\pi\sigma^2}}\int_{-\infty}^{M} e^{-\frac{(x-\mu)^2}{2\sigma^2}}dx, \tag{3}$$

where the parameter μ indicates the magnitude where earthquakes are detected at a rate of 50% and $\sigma(\sigma > 0)$ represents the range of magnitudes where earthquakes are more or less partially detected (Ogata and Katsura, 1993). The two parameters can generally be combined to describe the completeness of earthquake catalogs. Specifically, the minimum magnitude of completeness, M_C, can be approximately expressed using $\mu + 2\sigma$ or $\mu + 3\sigma$, which represents the complete record of magnitude at the 95.44% or 99.74% confidence level, respectively (Mignan and Woessner, 2012; Iwata, 2013).

Given a set of magnitudes $\{M_1, M_2, \ldots, M_n\}$, the seismic probability density function and the log-likelihood function can be written as:

$$\begin{aligned} P\left(M|\beta,\mu,\sigma\right) &= \frac{e^{-\beta M}q\left(M|\mu,\sigma\right)}{\int_{-\infty}^{+\infty} e^{-\beta M}q\left(M|\mu,\sigma\right)dM} \\ &= e^{-\beta M}q\left(M|\mu,\sigma\right)/e^{\left(-\beta\mu+\beta^2\sigma^2/2\right)}/\beta \\ &= \beta e^{-\beta\left(M-\mu\right)-\beta^2\sigma^2/2}q\left(M|\mu,\sigma\right), \end{aligned} \tag{4}$$

$$\begin{aligned} \ln L(\theta) = n\ln\beta - \sum_{i=1}^{n}\left[\beta M_i - \ln q\left(M_i|\mu,\sigma\right)\right] \\ + n\beta\mu - \frac{n}{2}\beta^2\sigma^2. \end{aligned} \tag{5}$$

Furthermore, we can obtain the parameters β, σ, and the dynamic $\mu(t)$ by the 'state-space' model, as well as p, c, k, and their standard deviations (Omi et al., 2013) by the Omori–Utsu formula (Omori, 1894; Utsu, 1961). Finally, we forecast the number of aftershocks with magnitudes $M > M_p$ (here M_p represents the minimum forecasting magnitude), which would take place during an arbitrary time interval $[t_2, t_e]$:

$$N = \int_{t_2}^{t_e}\int_{M_p}^{\infty}\lambda(t, M)dtdM. \tag{6}$$

In the study of the 2022 M_S6.9 Menyuan earthquake sequence, we used the catalog provided by the China Earthquake Networks Center (37.6–37.9°N, 100.9–101.6°E) between 2022/01/08 and 2022/01/13. Statistically, the aftershock sequence of the M6.9 Menyuan earthquake included two $M \geq 5.0$ aftershocks, nine M4.0~4.9 earthquakes, and forty-one M3.0~3.9 earthquakes (Figure 1). Parameter fitting and aftershock forecasting were performed using the Omi-R-J model, from 0.05 days after the main shock until 5.15 days, with steps of 0.05 days, totaling 103 time periods. It can be seen from Figure 2 that the expected parameters of the early post-earthquake sequence (t_2 = 1.00 days) are β =1.927 ± 0.083, k = 0.004 ± 0.002, p = 0.900 ± 0.051, and c = 0.004 ± 0.002, where the parameter β was calculated from $\beta = \ln(10)\times b$. In order to illustrate the evaluation results, Figures 2B,D depict the forecasted occurrence rates of M>2.95 for two periods of 1.00~2.00 days and 1.00~4.00 days after the main shock. The observed earthquake numbers for the two time periods were both within the 95% confidence intervals of the forecasted numbers, and the score values were [0.4238, 0.7283] and [0.4009, 0.7067] by the N-test (Kagan and Jackson, 1995; Schorlemmer et al., 2007; Zechar, 2010), respectively.

The N-test was intended to measure how well the total number of forecasted earthquakes matched the number of events observed. We used a one-sided test with an effective significance value, α_{eff}, which is half of the intended significance value, α. In other words, we intended to maintain an error rate of α= 5% and to compare both δ_1 and δ_2 with a critical value of α_{eff} = 0.025. If δ_1 is less than α_{eff}, the forecast rate is too low (under-prediction) and if δ_2 is less than α_{eff}, the forecast rate is too high (over-prediction). To quantitatively investigate the accuracy of the forecasted occurrence rates of strong aftershocks for different target magnitudes, M_T = [3.0, 3.5, 4.0] of the M_S6.9 Menyuan earthquake sequence, the N-test method was used to evaluate the performance results (Figure 3). The gray vertical line denotes the connection between the δ_1 score and the δ_2 score. Black diamonds and blue squares represent the results of δ_1<0.025 and δ_2<0.025, respectively. There is no blue square (δ_2 <0.025) in Figure 3, which indicates that there was no over-prediction in the forecasting period. The Omi-R-J method shows good forecasting ability for early strong aftershocks, and the blank space indicates that the actual number of earthquakes was zero. Ignoring the influence of 'no earthquakes', there was no over-prediction forecasting. The Omi-R-J model had 9, 8, and 7 forecasting failures before and after the strong aftershocks of M_S5.2 with respect to M_T = [3.0, 3.5, 4.0]; thus, for complex earthquake sequences, the Omi-R-J model with good fitting performance has some limitations. Further analysis of the period of forecasting failure shows that before and after the M_S5.2 strong aftershock of January 12, there was

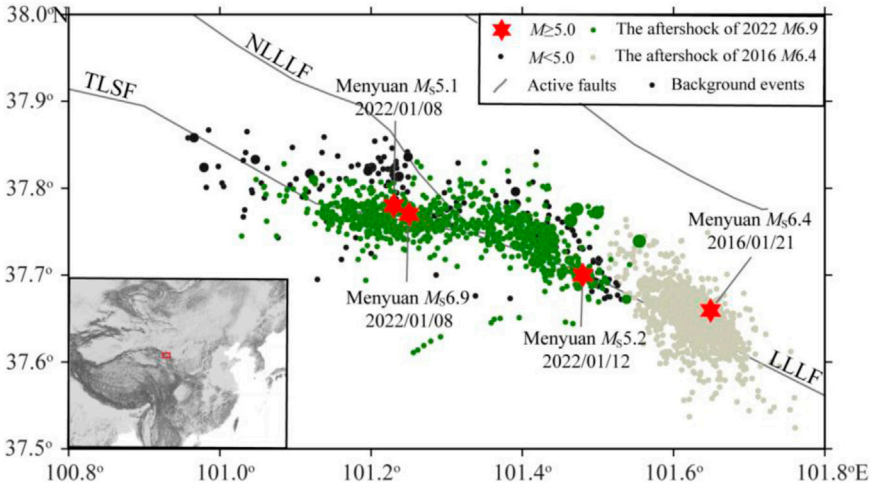

FIGURE 1
Spatial distribution of epicenters. The black dots represent background events before the Menyuan M_S6.9 since 1970. The gray dot represents the 2016 M_S6.4 Menyuan earthquake sequence, and the green dots represent the 2022 M_S6.9 Menyuan earthquake sequence. LLLF stands for Lenglongling fault, NTLSF is the north Lenglongling fault, and TLSF is the Tuolaishan fault.

obvious under-prediction forecasting, which coincides with the main period of forecasting failure.

Time-series *b*-value calculations based on a data-driven method

Data-driven technology provides a new solution to the problem of subjectivity of model selection in the calculation of seismicity parameters. In this paper, we utilized the time-sequence *b*-value data-driven (TbDD) method proposed by Jiang et al. (2021a) to analyze the M_S6.9 Menyuan earthquake sequence. The TbDD method consists of three major steps:

1) Selection of the magnitude–frequency distribution function. TbDD adopts the OK1993 model of a continuous distribution function given by Ogata and Katsura (1993) in a magnitude–frequency distribution relationship, which makes it superior by simultaneously determining the minimum magnitude of completeness and obtaining *b*-values.
2) Random partitioning in the time axis. In the model construction, it is necessary to randomly partition the given research time period $[t_0, t_1]$ between the start time, t_0, and the end time, t_1.① A random number generator was used to generate random time nodes, $T = \{T_1, T_2, \ldots, T_k\}$, where k is the number of time nodes. Correspondingly, the time period $[t_0, t_1]$ was divided into time segments $S = \{S_1, S_2, \ldots, S_{k+1}\}$, which constitute a model. ② We repeated step ① w times to obtain the w group partitioning schemes $\{P_i, i = 1, 2, \ldots, w\}$ on the time axis, that is, w models. ③ We repeated the aforementioned partitioning steps ① and ② with increasing k from 1 to n, where n is the maximum number of time nodes. For the time segments $S = \{S_1, S_2, \ldots, S_{k+1}\}$ of each model (or each partitioning scheme), the parameters of the OK1993 model $[\beta, \mu, \sigma]$ can be calculated using the events included in each time segment, and the total number of calculations was $w\times(n+1)$ times.

For any moment t_i in the time interval (t_0, t_1), the *b*-value is derived from the events both before and after t_i. For the moment t_0, the *b*-value is calculated by using only the events after t_0, and for the moment t_1, the *b*-value is obtained by using only the events before t_1. Therefore, only at the moment of t_1, the TbDD method has the characteristic of forward-forecasting. As time continues to move forward, the *b*-value at the original t_1 will be changed and updated.

3) Selection of the optimal models and calculation of ensemble median *b*-values. In order to select the optimal models most likely to reflect the final calculation results among a large number of models, the TbDD method adopted Bayesian information criteria (BIC) (Schwarz, 1978):

$$BIC = -2 \cdot \ln L(\theta) + k \cdot \ln(N), \tag{7}$$

where $\ln L(\theta)$ is the log-likelihood value of the OK1993 model given by formula (5), k is the degrees of freedom of the model, and N is the number of events for calculation. Because BIC is a penalized log-likelihood function, the smaller that BIC is, the closer to the true value the estimated parameters are. We ranked the BIC values of all the models obtained using Eq. 7 and selected the 5% models with

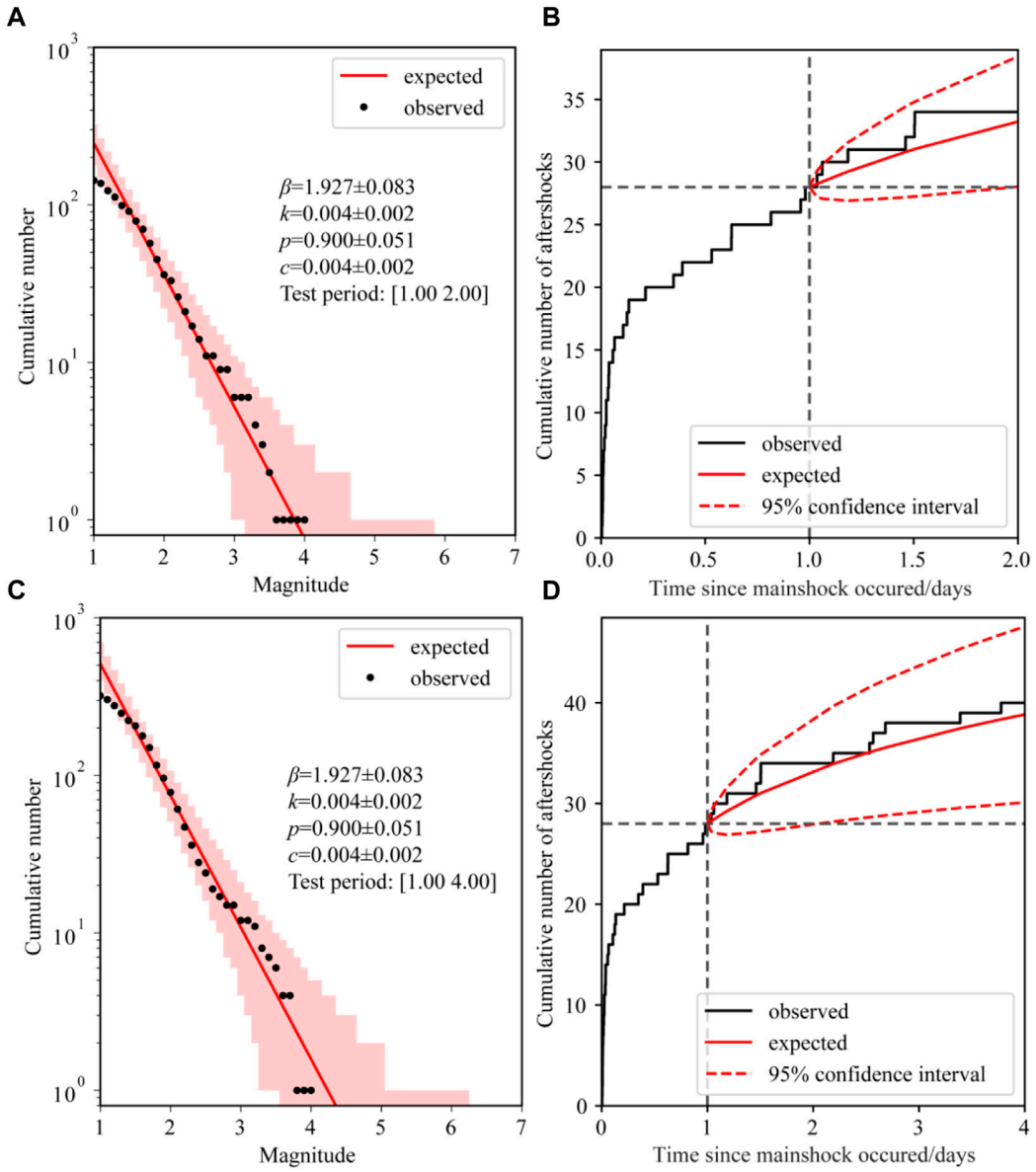

FIGURE 2
Future 1-day and 3-day aftershock forecasting for the Menyuan M_S6.9 earthquake sequence using the Omi-R-J model. **(A,B)** Time period of 1.00–2.00 days and **(C,D)** time period of 1.00–4.00 days after the main shock. **(A,C)** Comparison of magnitude–cumulative frequency between forecasting (red lines) and actual observed aftershocks (black dots) and their 95% confidence intervals (pink areas). **(B,D)** Comparison of magnitude–cumulative frequency between forecasting (red curves) and actual observed aftershocks (black curves) of M>2.95 and their 95% confidence intervals (red dashed lines), and the forecasting starting and ending times (black vertical dashed lines) are delineated.

minimum BIC values as the optimal ones. We used these optimal models to form an ensemble model and obtained the ensemble median b-value of the time-sequence as the final result. The median absolute deviation (MAD) was used as the uncertainty of the b-value.

We implemented TbDD to calculate the b-values of the M_S6.9 Menyuan earthquake sequence, attempting to use different maximum time segments (n+1) and different partitioning times (w). The models with the 5% lowest BIC values were taken as the optimal models, and the ensemble median values of the b-values were calculated as the final result. The BIC value distribution and the b-values of time sequences with the number of time segments $n + 1 = \{2,3,...11\}$ and $w = 100$ are shown in Figures 4A,B, separately. For the partitioning with $n + 1 =$

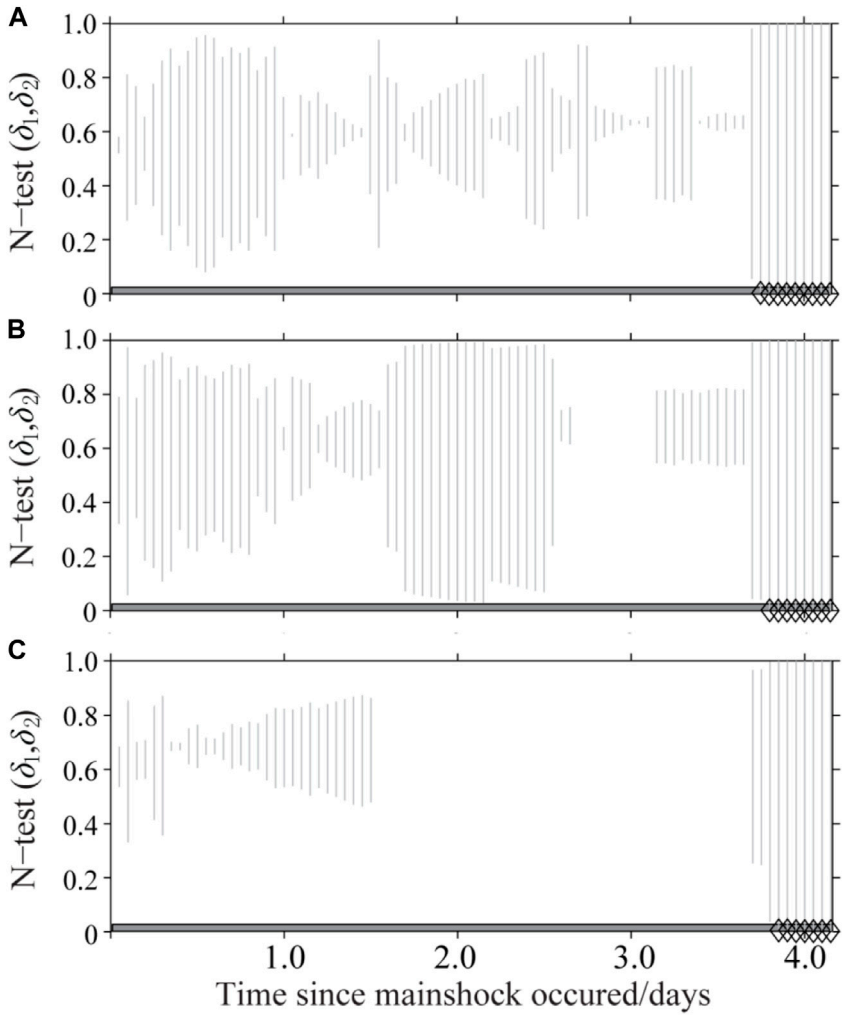

FIGURE 3
N-test results for future 1-day aftershock forecasting of the Menyuan M_S6.9 earthquake sequence. **(A–C)** Forecasting performance evaluation of the Omi-R-J model for the three target magnitudes, 3.0, 3.5, 4.0, respectively. The vertical gray dashed lines connect the δ_1 and δ_2 values, while the black diamonds and blue squares show the results with δ_1<0.025 and δ_2<0.025, respectively. The blank area indicates that no event of corresponding magnitudes have occurred in the forecasting period.

{2,3,...21} and w = 300, the results are shown in Figures 4C,D and for the partitioning with n + 1 = {2,3,...21} and w = 1000, the results are shown in Figures 4E,F. From the aforementioned calculation results, it can be seen that the b-values obtained under different combinations of maximum time segments (n + 1) and various partitioning times w are relatively close, which confirms the stability of the TbDD method. It is worth noting that, from 1.3 days before the January 12 M_S5.2 strong aftershock, the b-value dropped significantly, from b = 0.93 to b = 0.63, with a drop as high as $\triangle b$ = 0.30, which is the only time that the b-value of aftershocks dropped significantly over the study period. This phenomenon makes it possible to give an alarm before this strong aftershock.

SATLS for determining the risk level of strong aftershocks

To obtain a general threshold standard for the b-value changes of time series of strong aftershock risk alerts, which we used as a reference to conduct the strong aftershock forecasting of the M_S6.9 Menyuan earthquake sequence, we studied the b-value changes of time series before strong aftershocks of M≥5.0 based on 86 intraplate earthquake sequences in the China continent whose main shock had a magnitude of M_S≥6.0, as screened by Bi *et al.* (2022).We used the National Unified Official Catalogue produced by the China Earthquake Networks Center (CENC). Since 1 January 1970, the catalog has provided earthquake locations, occurrence

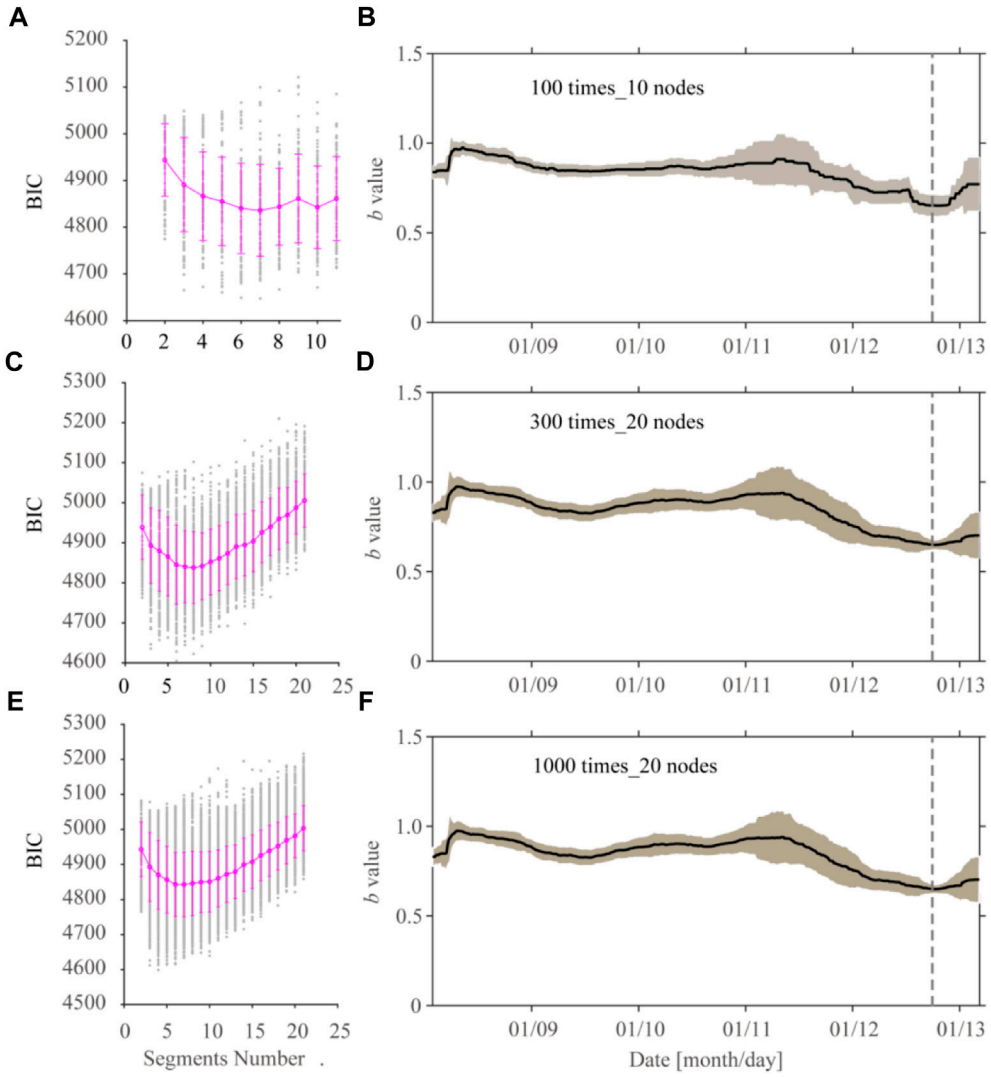

FIGURE 4
TbDD method calculation results for the 8 January 2022 Menyuan M_S6.9 earthquake sequence. **(A,C,E)** BIC value distribution under different partition periods. The gray dots denote the calculation results of BIC values, and the pink dots and vertical lines denote the corresponding means and standard deviations of the BIC values, respectively. **(B,D,F)** Time-sequence changes of *b*-values calculated by TbDD. The black curves indicate the ensemble medians of *b*-values, the gray areas indicate the MAD of corresponding *b*-values, and the gray vertical dotted lines show the time of occurrence of strong aftershocks of the Menyuan M_S5.2 aftershock on 12 January 2022.

times, and local magnitudes, M_L, obtained using the same formula (Mignan et al., 2013). Thus the homogeneity of the reported magnitude was ensured for the whole period. Since the National Unified Official Catalogue starts from 1970, earthquakes were selected from the period between 1970/01/01 and the time immediately before each of 86 main shocks, as well as spatial restrictions on the distribution of aftershocks. Then we used the Gardner–Knopoff method (Gardner and Knopoff, 1974) to decluster catalogs to obtain the background seismicity of the corresponding earthquake sequence. Because of the absence of a large number of aftershock events in the early post-earthquake period, which seriously affected the stability of model parameters, only the events from 0.50 days after the main shock to the occurrence of the strongest aftershock were used to ensure the stability and quality of parameter fitting. Additionally, both the number of background events and aftershocks of the selected earthquake sequence amounted to no fewer than 30 results in a total of 34 earthquake sequences. The parameters of 34 main shocks are shown in Table 1, and the spatial distribution of the epicenters of the main shocks is mapped in Figure 5A.

The parameters of 34 earthquake sequences were fitted using the OK1993 model, and the *b*-values of both background events

TABLE 1 Sequence parameters of intraplate earthquakes built for the SATLS in the China continent.

No.	Date	Time	Long	Lat	Mag	Mm	N_{bg}	N_{after}	b_{bg}	b_{after}
1	1976/11/07	02:04:05	101.08	27.50	6.7	4.9	0089	0730	1.01	1.02
2	1979/07/09	18:57:23	119.25	31.45	6.0	5.2	0057	0037	0.71	0.58
3	1981/01/24	05:13:47	101.17	31.00	6.9	4.3	0042	0055	0.85	0.91
4	1982/06/16	07:24:29	99.85	31.83	6.0	3.0	0299	0183	1.12	1.08
5	1985/08/23	20:41:55	75.32	39.53	7.1	6.6	0074	0048	1.00	0.93
6	1991/02/25	22:30:25	79.00	40.33	6.5	4.9	0117	0041	0.74	0.76
7	1996/07/03	14:44:44	88.60	30.25	6.0	5.4	0080	0047	0.78	0.76
8	1998/08/27	17:03:33	77.13	39.82	6.4	5.1	0759	0089	0.90	0.60
9	2001/10/27	13:35:40	100.57	26.23	6.0	4.1	0198	0069	0.65	0.96
10	2003/07/21	23:16:30	101.23	25.95	6.2	4.9	0283	0149	0.89	1.36
11	2003/10/16	20:28:03	101.30	25.92	6.1	5.1	0369	0223	1.00	1.08
12	2003/10/25	20:41:36	100.93	38.35	6.1	4.3	0047	0261	0.78	0.89
13	2005/02/15	07:38:07	79.37	41.72	6.2	5.1	0318	0036	0.86	0.78
14	2007/06/03	05:34:56	101.02	23.05	6.4	5.1	1656	0224	1.00	0.87
15	2008/05/12	14:28:04	103.40	31.00	8.0	6.4	2487	3014	0.86	1.25
16	2008/08/30	16:30:51	101.92	26.28	6.1	5.6	0247	0035	0.93	0.73
17	2008/11/10	09:21:59	95.91	37.66	6.6	5.3	0053	0116	0.70	0.68
18	2009/08/28	09:52:06	95.90	37.60	6.6	6.1	0144	0437	0.85	0.73
19	2012/06/30	05:07:31	84.74	43.42	6.6	4.6	0266	0298	0.76	0.88
20	2013/01/29	00:38:52	79.75	42.55	6.3	4.0	0074	0244	0.83	0.86
21	2013/04/20	08:02:47	102.99	30.30	7.0	5.4	0415	0188	0.99	0.87
22	2013/07/22	07:45:56	104.21	34.54	6.7	4.1	0202	0279	0.75	0.78
23	2013/08/12	05:23:42	97.96	30.04	6.1	4.1	0089	0113	0.91	0.97
24	2014/02/12	17:19:48	82.51	36.14	7.3	4.5	0060	0483	0.70	1.00
25	2014/05/30	09:20:13	97.80	25.02	6.1	4.6	3840	2974	0.88	1.02
26	2014/08/03	16:30:12	103.33	27.11	6.6	4.4	0677	1514	1.16	1.11
27	2016/01/21	01:13:12	101.65	37.66	6.4	4.1	0374	0425	0.85	0.81
28	2016/10/17	15:14:47	95.02	32.89	6.3	4.4	0063	0526	0.70	0.95
29	2016/12/08	13:15:03	86.30	43.80	6.2	4.6	0982	0879	0.72	0.83
30	2017/08/08	21:19:48	103.82	33.20	7.0	4.3	4503	4884	0.80	0.86
31	2017/11/18	06:34:18	95.00	29.75	6.9	4.3	0131	2749	0.77	1.17
32	2019/06/17	22:55:43	104.96	28.34	6.0	5.6	3194	1800	0.73	0.73
33	2020/01/19	21:27:56	77.21	39.83	6.4	4.8	0542	1077	0.72	0.86
34	2020/06/26	05:05:19	82.34	35.69	6.4	4.9	0282	0539	0.85	0.79

(b_{bg}) and aftershocks (b_{after}) are shown in Table 1. Statistical analyses indicated 13 earthquake sequences with M≥5.0 aftershocks. The average was b_{bg} = 0.87 ± 0.11 and b_{after} = 0.81 ± 0.19, and b_{bg}>b_{after} accounted for 84.62% (11/13) and b_{bg}<b_{after} accounted for 15.38% (2/13); there were 21 earthquake sequences without strong M≥5.0 aftershocks in the fitting period, with average b_{bg} = 0.83 ± 0.13 and b_{after} = 0.95 ± 0.15, of which b_{bg}>b_{after} accounted for 19.05% (4/21) and b_{bg}<b_{after} accounted for 80.95% (17/21). The statistical distribution of the differences in b-values between the background events b_{bg} and the aftershocks b_{after}, ($\triangle b$ = b_{after} - b_{bg}), and the ratio $\triangle b/b_{bg}$ are given in Figures 5B,C. The results show that the mean $\triangle b$ value and the median $\triangle b$ value of the sequences having strong aftershocks of M≥5.0 were −0.13 and −0.16, separately, and that the mean and the median of $\triangle b/b_{bg}$ were −0.06 and −0.08, separately. However, the $\triangle b$ of the sequences without strong aftershocks of M≥5.0 had a mean value of 0.27 and a median value of 0.15, and the mean value of $\triangle b/b_{bg}$ was 0.16 and the median value was 0.08.

The aforementioned analysis shows that b_{after}<b_{bg} for the sequences with M≥5.0 aftershocks and b_{after}>b_{bg} for the sequences without M≥5.0 aftershocks are statistically significant. If we conduct the risk assessment of M≥5.0 aftershocks according to the aforementioned relationship, it can be seen that when $\triangle b$>0, two earthquake

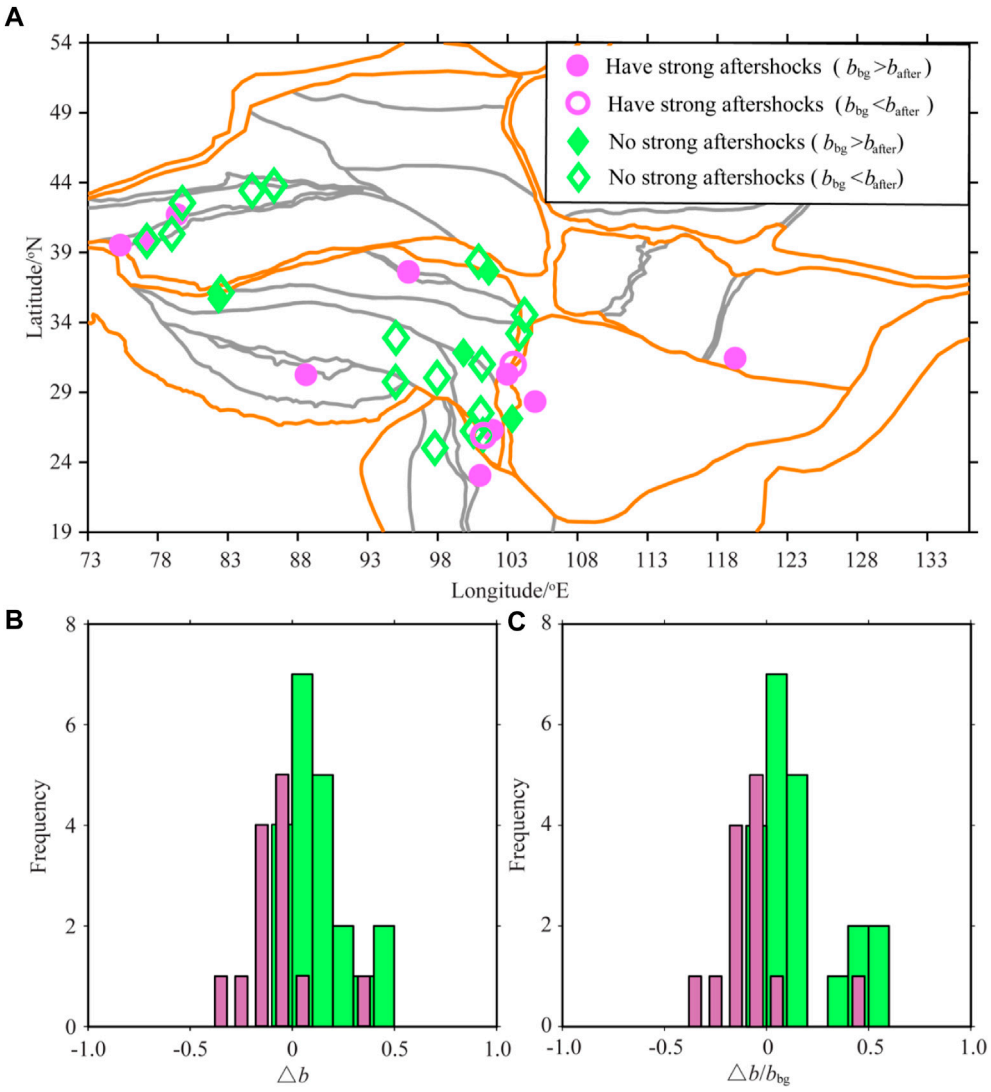

FIGURE 5
Distribution characteristics of 34 M_S≥6.0 earthquake sequences in the China continent. **(A)** Distribution of the epicenters of the main shocks. They are classified according to the presence or absence of strong aftershocks of M≥5.0 and the relative size relationship between b-values of background events (b_{bg}) and that of aftershocks (b_{after}), and indicated by different colors. The brown represents the boundary line of the primary plate, and the gray represents the boundary line of the secondary plate. **(B)** Statistical distribution of differences between background events b_{bg} and aftershock b_{after}, $\triangle b$. **(C)** Statistical relationship of $\triangle b/b_{bg}$. In **(B,C)**, light red represents the earthquake sequences having strong aftershocks of M≥5.0, and light green represents the earthquake sequences having no strong aftershocks of M≥5.0.

sequences have M≥5.0 aftershocks, and 17 earthquake sequences have no aftershocks with M≥5.0; when $\triangle b$<0, eleven earthquake sequences have M≥5.0 aftershocks, and four earthquake sequences have no aftershocks with M≥5.0. Furthermore, when $\triangle b$>0.1, only one earthquake event had aftershocks of M≥5.0, while when $\triangle b$<-0.1, all earthquake sequences had aftershocks of M≥5.0. The statistical results are illustrated in Figure 6A. This shows that the possibility of strong aftershocks with M≥5.0 can be reliably determined by defining $\triangle b$=±0.1. Moreover, from Figure 6A, when $\triangle b$<0, especially $\triangle b$<-0.1, the magnitude difference between a main shock and its largest aftershock mainly ranged from 0 to 1.5. While, when $\triangle b$>0, the magnitude difference ranged from 1.5 to 3.0.

The earthquake monitoring capability of the China Earthquake Networks Center was significantly improved after the 2008 M_S8.0 Wenchuan earthquake (Huang et al., 2017). To eliminate the influence of the change in earthquake monitoring capability, we excluded the earthquake sequences before the 2008 M_S8.0 Wenchuan earthquake and investigated the relationship between $\triangle b$ and the occurrence of strong

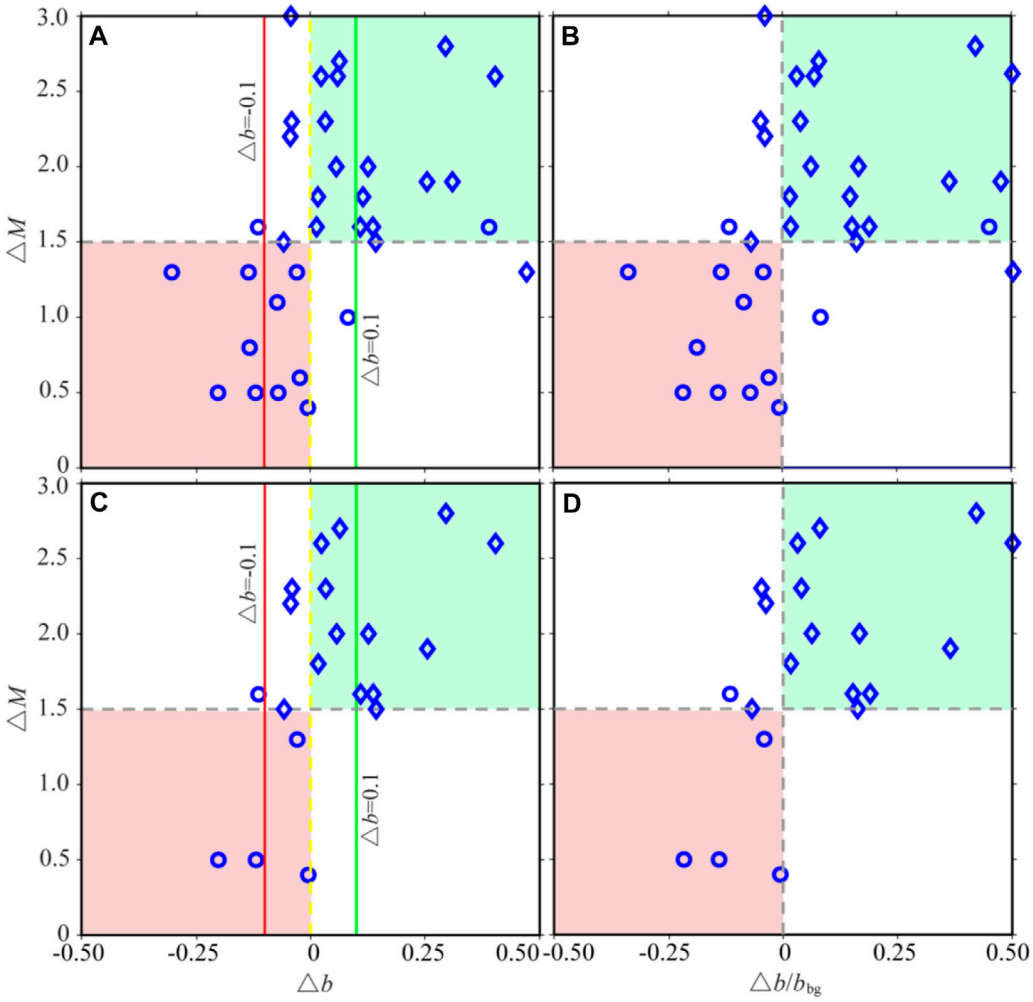

FIGURE 6
Relationship between magnitude difference and sequence parameters. **(A)** Relationship between $\triangle M$ and $\triangle b$ ($\triangle b = b_{after} - b_{bg}$) (1970.01.01–2020.07.30); **(B)** relationship between $\triangle M$ and $\triangle b/b_{bg}$ (1970.01.01–2020.07.30); **(C)** relationship between $\triangle M$ and $\triangle b$ of the sequences after 12 May 2008; **(D)** relationship between $\triangle M$ and $\triangle b/b_{bg}$ of the sequences after 12 May 2008. The circle represents the earthquake sequence having strong aftershocks with $M \geq 5.0$, and the diamond represents the earthquake sequence having no strong aftershocks with $M \geq 5.0$ in the fitting period. The red, yellow, and green lines indicate $\triangle b = 0.1$, $\triangle b = 0$ and $\triangle b = -0.1$, respectively. The green area represents $\triangle M > 1.5$ and $\triangle b > 0$, while the red area represents $\triangle M < 1.5$ and $\triangle b < 0$.

aftershocks of $M \geq 5.0$. The results demonstrate that all earthquake sequences have no strong aftershocks with $M \geq 5.0$ when $\triangle b > 0.1$, while when $\triangle b < -0.1$, all earthquake sequences have strong aftershocks with $M \geq 5.0$ (Figure 6C). In addition, we also used $\triangle b/b_{bg}$ for similar analyses, and found the same risk classification effectiveness using $\triangle b/b_{bg} = \pm 0.1$ as using $\triangle b = \pm 0.1$, as shown in Figures 6B,D.

Based on the aforementioned calculations, we defined $\triangle b = 0.1$ as the green threshold with low risk of $M \geq 5.0$ strong aftershocks, that is, when $\triangle b \geq 0.1$, the possibility of $M \geq 5.0$ strong aftershocks is low; $\triangle b = -0.1$ is a high-risk red threshold for strong aftershocks with $M \geq 5.0$. When $\triangle b$ is lower than this threshold, that is $\triangle b \leq -0.1$, the possibility of strong aftershocks with $M \geq 5.0$ is high; $\triangle b = 0$ represents a distinct yellow threshold. When $-0.1 < \triangle b < 0.1$, we should pay attention to the occurrence of strong $M \geq 5.0$ aftershocks. By combination with the TbDD method based on data-driven technology to calculate b_{bg}, b_{after}, and $\triangle b$, a strong aftershock traffic light system (SATLS) was constructed to accurately determine the risk of strong $M \geq 5.0$ aftershocks in real time, which makes it feasible to make targeted disaster mitigation decisions.

We performed SATLS classification of the occurrence of strong aftershocks with $M \geq 5.0$ for the 2022 M_S6.9 Menyuan earthquake sequence followed by only two aftershocks of $M \geq 5.0$. The M_S5.1 aftershock occurred within just a few hours after the main shock, and the poor data availability

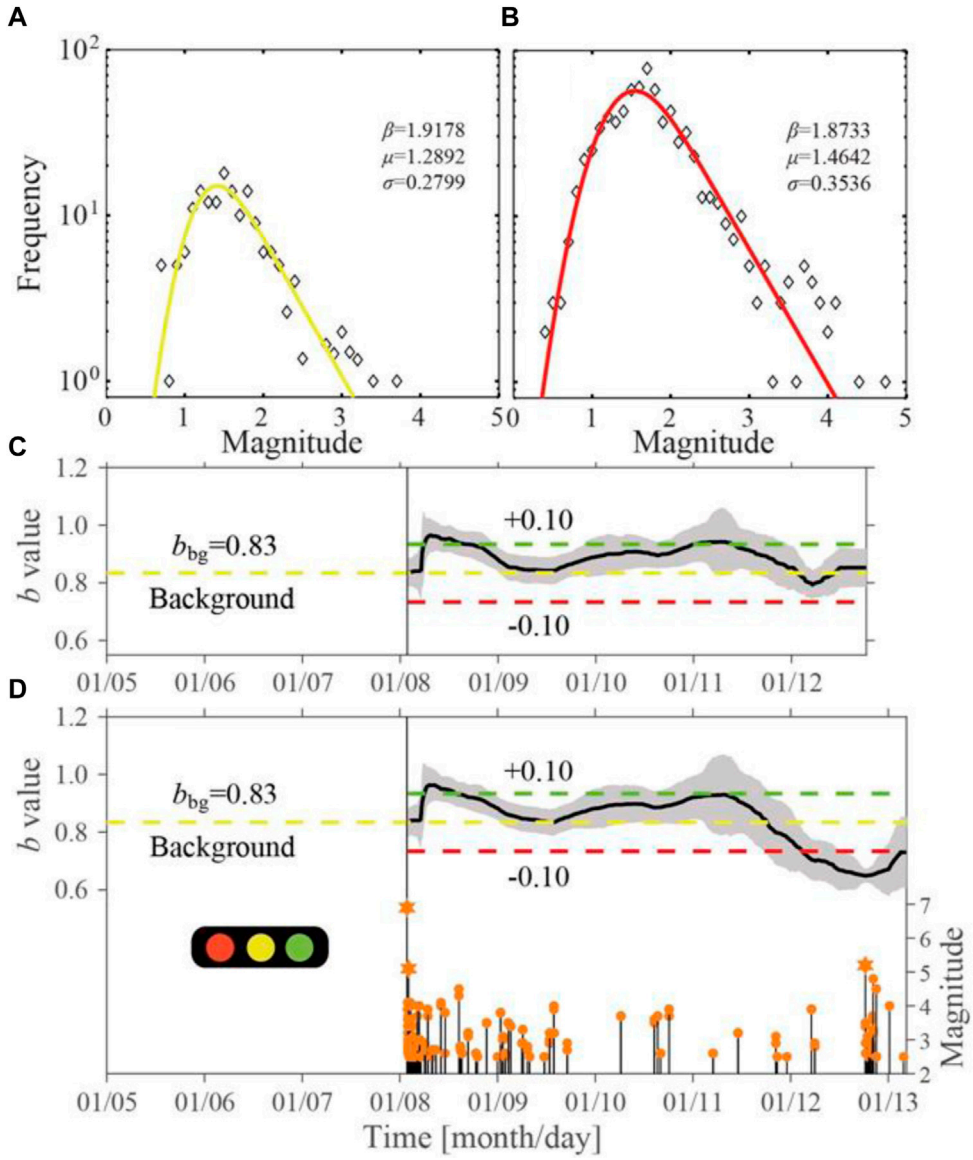

FIGURE 7
Characteristics of the *b*-value evolution for the 8 January 2022 Menyuan M_S6.9 earthquake sequence and SATLS settings. **(A,B)** Magnitude–frequency distribution (FMD) and the fitting results of the OK1993 model. They correspond to the background earthquake sequence (1970.01.01~2022.01.08) and aftershock sequence (2022.01.08~2022.01.12), respectively. The diamonds denote the FMD of the events. The solid curve indicates the fitting results of the OK1993 model, and the actual parameters are marked in each subgraph in the order of β, μ, and σ. **(C)** *b*-value of time series obtained using the events immediately before the strong aftershock (2022.01.08~2022.01.12). **(D)** *b*-value of time series calculated using the events between the main shock and the time after the strong aftershock (2022.01.08~2022.01.13). The yellow dotted line indicates background value b_{bg} (yellow threshold), the red dotted line denotes the red threshold (0.1 lower than the background value), the green dotted line represents the green threshold (0.1 higher than the background value), and the magnitude–time distribution (*M*-*t*) of the earthquake sequence is displayed.

before this event may result in large uncertainties in the *b*-values. Therefore, only the January 12 M_S5.2 aftershock was discussed here. The data for calculation were obtained from the National Unified Official Catalogue, and the spatial range covered was the same as the distribution of aftershocks. The events from 1970 to the time before the main shock were taken as background events, and those between the main shock and the M_S5.2 aftershock were taken as aftershock sequences.

The results showed that b_{bg} = 0.83 and b_{after} = 0.81, and the corresponding fitting curves of the OK1993 model are shown in Figures 7A,B. Because $b_{after}<b_{bg}$, it can be determined that the

yellow threshold of SATLS has been reached. The *b*-values of the time series were calculated by TbDD as shown in Figure 7C. Before the M_S5.2 aftershock, the *b*-value had dropped to about 0.79, that is, $\triangle b \approx$-0.04, according to which a yellow alert for the possibility of a strong aftershock with $M \geq 5$ would be declared.

We further investigated the *b*-values of the time-series between the main shock and the time after the M_S5.2 aftershock as shown in Figure 7D. The results indicated that before the M_S5.2 strong aftershock, the *b*-value decreased to about 0.63, $\triangle b \approx$-0.2, the magnitude of which is larger than that of $\triangle b \approx$-0.04, as obtained using events between the main shock and the M_S5.2 aftershock. After the M_S5.2 strong aftershock, the stress around the focal area changed and the *b*-value continued to decrease. Yang et al. (2022) obtained the background *b*-value of 0.84 using the maximum-likelihood method and the whole aftershock *b*-value of 0.67 using the least-squares method for the Menyuan earthquake, and our results were similar to theirs. The *h*-value is a constant in the revised Omori's law which describes the number of aftershocks after the main shock. It can be used to determine whether there might be future events with larger magnitudes during an ongoing sequence (Liu et al., 1979). If $h \gg 1$, it indicates that the largest magnitude earthquake already occurred as the main shock. If $h \ll 1$, then it was considered a foreshock sequence. The 2022 Menyuan sequence showed that the overall *h*-value was significantly larger than 1. (Yang et al., 2022).

Discussion

The SATLS proposed in this paper is, in a more general sense, an extension of the FTLS which determined whether an event was a main shock or a foreshock to an even stronger event yet to come. However, there are several limitations to the SATLS. First, the threshold settings of the SATLS are only based on a limited number of earthquake cases, and it is only suitable for the intraplate earthquake sequences of the $M \geq 6.0$ main shock in the China continent followed by $M \geq 5.0$ aftershocks. Moreover, there is a lack of systematic and comprehensive understanding of the relative relationship between the values of b_{after} and b_{bg} in different tectonic regions, which limits the general applicability of the SATLS. In addition, some researchers argue that the spatial distribution of *b*-values is highly variable. For example, the ductile shear zone has a higher *b*-value than the brittle-ductile shear zone (Villiger et al., 2020). Also, it is easy for a high *b*-value to be produced in rocks with low Young's modulus (Zorn et al., 2019) or high organic content, which causes difficulties in the application of SATLS for earthquake sequences with large-scale spatial distribution in aftershock zones, and it may be necessary to develop a set of two-dimensional time-space $\triangle b$ risk classification thresholds. There are also some shortfalls in this research. Thirty-four events may not be enough to derive exact thresholds. With respect to the whole *b*-value calculated by the OK1993 model, the uncertainty and the confidence interval of the whole *b*-value has not been resolved, which needs to be addressed in subsequent research.

During revision of this paper, there occurred in China on 5 September 2022, the M_S6.8 Luding earthquake with an M_S5.0 aftershock, which provided a new opportunity to verify the effectiveness of the SATLS. Therefore, along with the Menyuan earthquake, we also applied SATLS to the M_S6.8 2022 Luding earthquake sequence. We obtained b_{bg} = 0.9672 from the OK1993 model and *b*-values of time series by TbDD. The results showed that three days before the M_S5.0 earthquake, the *b*-value started to decrease. As of 13: 17 on October 23 when the M_S5.0 aftershock occurred, the *b*-value had decreased to about 0.86, for a $\triangle b \approx$ -0.1, which suggests that a red alert could have been declared for a strong aftershock of $M \geq 5.0$. To some extent, this event demonstrates the effectiveness of SATLS.

Although the N-test results showed that the Omi-R-J model failed in forecasting the strong M_S5.2 aftershock, the failure reason could not rule out the possibility that the Omi-R-J method is based on the Omori–Utsu formula with a relatively simple aftershock attenuation law, and it only demonstrates obvious forecasting effectiveness for aftershock sequences with underdeveloped secondary aftershocks. For more complex earthquake sequences, the analysis may need to be combined with the ETAS model. In fact, CSEP also focuses on the predictability of some huge earthquake cases (Schorlemmer et al., 2018). For example, after the 2011 *M*9.0 earthquake in East Japan, Nanjo *et al.* (2012) and Ogata *et al.* (2013) systematically tested the forecasting effectiveness of various versions of the ETAS model and confirmed that it showed good forecasting performance on complex aftershock sequences. In the future, a combination of the semi-quantitative and semi-qualitative SATLS and the quantitative statistical probability forecasting models is still a realistic and feasible choice.

Conclusion

It is difficult to accurately forecast a disaster-causing aftershock using only traditional statistical forecasting models. We first used the TbDD method based on data-driven technology to obtain reliable *b*-values of time series. Second, based on the empirical relationship, $\triangle b = b_{after} - b_{bg}$, from 34 $M \geq 6.0$ intraplate earthquake sequences in the China continent and their strongest aftershocks of $M \geq 5.0$, a strong aftershock traffic light system (SATLS) was constructed. Taking the 8 January 2022 M_S6.9 Menyuan earthquake in Qinghai Province as an example, a yellow alert attempt was made by using SATLS for the M_S5.2 strong aftershocks that occurred several days after the main shock. The main results are summarized as follows:

1) The Omi-R-J model for aftershock probability forecasting was employed to conduct 83 consecutive sliding forecasts of strong aftershocks of the M_S6.9 Menyuan earthquake sequence, and the forecasting performance was assessed by the N-test method. The results showed that the earthquake occurrence rates forecast by the Omi-R-J model before the largest aftershock (M_S5.2) were too low; however, the model can accurately forecast aftershock rates for each magnitude interval in most time-periods, which makes it difficult to accurately forecast this strong aftershock.
2) The data from our research on the 34 M≥6.0 intraplate earthquake sequences in the China continent showed that $\triangle b = b_{after} - b_{bg} = \pm 0.1$ can act as a discriminator to determine whether strong aftershocks of magnitude 5.0 or higher will occur. If the difference ($\triangle b = b_{after} - b_{bg}$) exceeded +0.1 ($\triangle b$ = 0.1) or was -0.1 ($\triangle b$ = -0.1), we assigned a traffic light color of green or red, respectively, otherwise yellow. We can further infer the possible magnitude of an aftershock based on the relationship between $\triangle M$ and $\triangle b$.
3) The b-value calculation of the M_S6.9 Menyuan earthquake sequence using TbDD showed that, for different time partitioning schemes, random partitioning times, and other technical rules, the perturbation of determined time series b-values was negligible. The b-value obtained using the events between the main shock and the M_S5.2 event decreased 0.04 ($\triangle b \approx$ -0.04) from 1.3 days before the M_S5.2 strong aftershock, while the b-value calculated using the events between the main shock and the time after the M_S5.2 earthquake decreased 0.2 and gradually recovered after this strong aftershock. From the time-series of b-values of the 2022 M_S6.9 Menyuan earthquake sequence, before the M_S5.2 event, only a yellow alert could be declared, which shows a gap from the expected determined red alert. One reason may be that it is questionable if the seismicity before an M≥5.0 strong aftershock could reveal the stress status of that moment. The fact that a strong aftershock of M≥5.0 abruptly changes the stress status in the focal area may be another factor. To improve the accuracy of forecast making, a deeper understanding of the true b-value and the detailed description of the stress evolution state in the source area is needed.(Gutenberg and Richter, 1944; Nandan et al., 2017; Si and Jiang, 2019; Jiang et al., 2021).

Data and resources

The earthquake catalog used in this paper was provided by the China Earthquake Networks Center. The Multi-Parametric Toolbox 3.0 (https://www.mpt3.org/Main/HomePage, last accessed February 2022) is used for the analysis of parametric optimization.

Data availability statement

The original contributions presented in the study are included in the article/Supplementary Material, and further inquiries can be directed to the corresponding author.

Author contributions

JB, FY, and CJ contributed to conceptualization. JB prepared the manuscript with contributions from all authors. JB, FY, and CJ wrote software for data processing. XY, YM, and CS contributed to the revised manuscript version.

Funding

This study was supported by the Joint Funds of the National Natural Science Foundation of China and the Foundation of Earthquake Science (U1839207), the Special Fund of the Institute of Geophysics, China Earthquake Administration (DQJB22Z01) and the 2022 Earthquake Regime Tracking Work of the CEA (2022010116).

Acknowledgments

The authors thank Yan Zhang and Hongyu Zhai of the Institute of Geophysics, China Earthquake Administration, for their constructive suggestions on this paper. We also thank the editor and two anonymous reviewers for their very helpful comments and suggestions. This study used the National Unified Official Catalogue provided by the China Earthquake Networks Center.

Conflict of interest

The authors declare that the research was conducted in the absence of any commercial or financial relationships that could be construed as a potential conflict of interest.

Publisher's note

All claims expressed in this article are solely those of the authors and do not necessarily represent those of their affiliated organizations, or those of the publisher, the editors, and the reviewers. Any product that may be evaluated in this article, or claim that may be made by its manufacturer, is not guaranteed or endorsed by the publisher.

References

Bi, J. M., and Jiang, C. S. (2020). Comparison of early aftershock forecasting for the 2008 Wenchuan M_S8.0 earthquake. *Pure Appl. Geophys.* 177, 9–25. doi:10.1007/s00024-019-02192-6

Bi, J. M., Jiang, C. S., Lai, G. J., and Song, C. (2022). Effectiveness evaluation and constraints of early aftershock probability forecasting for strong earthquakes in continental China. *Chin. J. Geophys.* (in Chinese) 65 (7), 2532–2545. doi:10.6038/cjg2022P0411

Bi, J. M., Jiang, C. S., and Ma, Y. (2020). The study on early sequence parameters and probability forecasting of strong aftershocks of Changning M_S6.0 earthquake on June 17, 2019, Sichuan Province. *Earthquake* (in Chinese) 40 (2), 140–154. doi:10.12196/j.issn.1000-3274.2020.02.011

Chan, L. S., and Chandler, A. M. (2001). Spatial bias in *b*-value of the frequency–magnitude relation for the Hong Kong region. *Journal of Asian Earth Sciences* 20 (1), 73–81. doi:10.1016/s1367-9120(01)00025-6

Gardner, J. K., and Knopoff, L. (1974). Is the sequence of earthquakes in Southern California with aftershocks removed, Poissonian? *Bulletin of the Seismological Society of America* 64, 1363–1367. doi:10.1785/bssa0640051363

Grimm, C., Käser, M., Hainzl, S., Pagani, M., and Kuchenhoff, H. (2021). Improving earthquake doublet frequency predictions by modified spatial trigger kernels in the Epidemic-Type Aftershock Sequence (ETAS) Model. *Bull. Seismol. Soc. Am.* 112 (1), 474–493. doi:10.1785/0120210097

Gulia, L., Rinaldi, A. P., Tormann, T., Vannucci, G., Enescu, B., and Wiemer, S. (2018). The effect of a mainshock on the size distribution of the aftershocks. *Geophys. Res. Lett.* 45, 13277–13287. doi:10.1029/2018GL080619

Gulia, L., and Wiemer, S. (2019). Real-time discrimination of earthquake foreshocks and aftershocks. *Nature* 574 (7777), 193–199. doi:10.1038/s41586-019-1606-4

Gulia, L., Wiemer, S., and Vannucci, G. (2020). Pseudoprospective evaluation of the foreshock traffic-light system in Ridgecrest and implications for aftershock hazard assessment. *Seismological Research Letters* 91 (5), 2828–2842. doi:10.1785/0220190307

Gutenberg, R., and Richter, C. F. (1944). Frequency of earthquakes in California. *Bulletin of the Seismological Society of America* 34, 185–188. doi:10.1785/bssa0340040185

Huang, F. Q., Li, M., Ma, Y. C., Han, Y., Tian, L., Yan, W., et al. (2017). Studies on earthquake precursors in China: A review for recent 50 years. *Geodesy and Geodynamics* 8 (1), 1–12. doi:10.1016/j.geog.2016.12.002

Iwata, T. (2013). Estimation of completeness magnitude considering daily variation in earthquake detection capability. *Geophysical Journal International* 194 (3), 1909–1919. doi:10.1093/gji/ggt208

Jiang, C., Qiu, Y., Jiang, C. S., Yin, X. X., Zhai, H. Y., Zhang, Y. B., et al. (2021a). A new method for calculating *b*-value of time sequence based on data-driven (TbDD): A case study of the 2021 yangbi M_S6.4 earthquake sequence in yunnan. *Chinese Journal of Geophysics (in Chinese)* 64 (9), 3126–3134. doi:10.6038/cjg2021P0385

Jiang, C., Jiang, C. S., Yin, F. L., Zhang, Y. B., Bi, J. M., Long, F., et al. (2021b). Traffic light system (TLS) for risk control of earthquake induced by industrial activities: Problem and prospects. *Progress in Geophysics* (in Chinese) 36 (6), 2320–2328. doi:10.6038/pg2021EE0495

Jiang, C. S., Bi, J. M., Wang, F. C., et al. (2018). Application of the Omi-R-J method for forecast of early aftershocks to the 2017 Jiuzhaigou, Sichuan, M_S7.0 earthquake. *Chinese Journal of Geophysics* (in Chinese) 61, 2099–2110. doi:10.6038/cjg2018M0113

Jiang, C. S., Han, L. B., Long, F., Lai, G., Yin, F., Bi, J., et al. (2021). Spatiotemporal heterogeneity of *b* values revealed by a data-driven approach for June 17, 2019 M_S 6.0, Changning Sichuan, China earthquake sequence. *Nat. Hazards Earth Syst. Sci.* 21, 2233–2244. doi:10.5194/nhess-21-2233-2021

Kagan, Y. Y., and Jackson, D. D. (1995). New seismic gap hypothesis: Five years after. *J. Geophys. Res.* 100 (B3), 3943–3959. doi:10.1029/94jb03014

Lippiello, E., Giacco, F., Marzocchi, W., Godano, G., and Arcangelis, L. d. (2017). Statistical features of foreshocks in instrumental and ETAS catalogs. *Pure Appl. Geophys.* 174 (4), 1679–1697. doi:10.1007/s00024-017-1502-5

Liu, Z. R., Qian, Z. X., and Wang, W. Q. (1979). Decay in earthquake frequency, an indicator of foreshocks. *Journal of Seismological Research* (in Chinese) 2 (4), 1–9.

Lv, X. J., Gao, M. T., Gao, Z. W., and Mi, S. T. (2007). Comparison of the spatial distribution of ground motion between mainshocks and strong aftershocks. *Acta Seismologica Sinica* (in Chinese) 29 (3), 295–301. doi:10.1007/s11589-007-0312-8

Matsu'ura, R. S. (1986). Precursory quiescence and recovery of aftershock activities before some large aftershocks. *Bulletin of the Earthquake Research Institute* 61, 1–65.

Mignan, A., Jiang, C. S., Zechar, J. D., Wiemer, S., Wu, Z., and Huang, Z. (2013). Completeness of the mainland China earthquake catalog and implications for the setup of the China earthquake forecast testing center. *Bulletin of the Seismological Society of America* 103 (2A), 845–859. doi:10.1785/0120120052

Mignan, A., and Woessner, J. (2012). Estimating the magnitude of completeness for earthquake catalogs. *CORSSA Community Online Resource for Statistical Seismicity Analysis*. doi:10.5078/corssa-00180805

Nandan, S., Ouillon, G., Wiemer, S., and Sornette, D. (2017). Objective estimation of spatially variable parameters of epidemic type aftershock sequence model: Application to California. *J. Geophys. Res. Solid Earth* 122 (7), 5118–5143. doi:10.1002/2016JB013266

Nanjo, K. Z., Izutsu, J., Orihara, Y., and Kamogawa, M. (2022). Changes in seismicity pattern due to the 2016 Kumamoto earthquake sequence and implications for improving the foreshock traffic-light system. *Tectonophysics* 822, 229175. doi:10.1016/j.tecto.2021.229175

Nanjo, K. Z., Tsuruoka, H., Yokoi, S., Ogata, Y., Falcone, G., Hirata, N., et al. (2012). Predictability study on the aftershock sequence following the 2011 Tohoku-Oki, Japan, earthquake: First results. *Geophys. J. Int.* 191, 653–658. doi:10.1111/j.1365-246X.2012.05626.x

Ogata, Y., and Katsura, K. (1993). Analysis of temporal and spatial heterogeneity of magnitude frequency distribution inferred from earthquake catalogues. *Geophys. J. Int.* 113 (3), 727–738. doi:10.1111/j.1365-246x.1993.tb04663.x

Ogata, Y., Katsura, K., Falcone, G., Nanjo, K., and Zhuang, J. (2013). Comprehensive and topical evaluations of earthquake forecasts in terms of number, time, space, and magnitude. *Bulletin of the Seismological Society of America* 103 (3), 1692–1708. doi:10.1785/0120120063

Ogata, Y. (2001). Increased probability of large earthquakes near aftershock regions with relative quiescence. *J. Geophys. Res.* 106, 8729–8744. doi:10.1029/2000jb900400

Ogata, Y. (2006). Monitoring of anomaly in the aftershock sequence of the 2005 earthquake of M7.0 off coast of the Western Fukuoka, Japan, by the ETAS model. *Geophys. Res. Lett.* 33, L01303. doi:10.1029/2005GL024405

Ogata, Y. (1989). Statistical model for standard seismicity and detection of anomalies by residual analysis. *Tectonophysics* 169 (1/2/3), 159–174. doi:10.1016/0040-1951(89)90191-1

Omi, T., Ogata, Y., Hirata, Y., and Aihara, K. (2013). Forecasting large aftershocks within one day after the main shock. *Sci. Rep.* 3, 2218. doi:10.1038/srep02218

Omi, T., Ogata, Y., Hirata, Y., and Aihara, K. (2015). Intermediate-term forecasting of aftershocks from an early aftershock sequence: Bayesian and ensemble forecasting approaches. *J. Geophys. Res. Solid Earth* 120 (4), 2561–2578. doi:10.1002/2014JB011456

Omi, T., Ogata, Y., Shiomi, K., Enescu, B., Sawazaki, K., and Aihara, K. (2016). Automatic aftershock forecasting: A test using real-time seismicity data in Japan. *Bulletin of the Seismological Society of America* 106 (6), 2450–2458. doi:10.1785/0120160100

Omori, F. (1894) Tokyo, Japan. Imperial University of Tokyo, 111–200.On aftershocks of earthquakes, Doctoral dissertation.

Reasenberg, P. A., and Jones, L. M. (1989). Earthquake hazard after a mainshock in California. *Science* 243, 1173–1176. doi:10.1126/science.243.4895.1173

Scholz, C. H. (2015). On the stress dependence of the earthquake *b*-value. *Geophys. Res. Lett.* 42 (5), 1399–1402. doi:10.1002/2014GL062863

Scholz, C. H. (1968). The frequency-magnitude relation of microfracturing in rock and its relation to earthquakes. *Bulletin of the Seismological Society of America* 58 (1), 399–415. doi:10.1785/bssa0580010399

Schorlemmer, D., Gerstenberger, M. C., Wiemer, S., Jackson, D. D., and Rhoades, D. A. (2007). Earthquake likelihood model testing. *Seismological Research Letters* 78, 17–29. doi:10.1785/gssrl.78.1.17

Schorlemmer, D., Werner, M. J., Marzocchi, W., Jordan, T. H., Ogata, Y., Jackson, D. D., et al. (2018). The collaboratory for the study of earthquake predictability: Achievements and priorities. *Seismological Research Letters* 89 (4), 1305–1313. doi:10.1785/0220180053

Schwarz, G. (1978). Estimating the dimension of a model. *Ann. Statist.* 6 (2), 461–464. doi:10.1214/aos/1176344136

Shcherbakov, R. (2021). Statistics and forecasting of aftershocks during the 2019 Ridgecrest, California, earthquake sequence. *J. Geophys. Res. Solid Earth* 126, e2020JB020887. doi:10.1029/2020JB020887

Si, Z. Y., and Jiang, C. S. (2019). Research on parameter calculation for the Ogata-Katsura 1993 model in terms of the frequency-magnitude distribution based on a data-driven approach. *Seismological Research Letters* 90 (3), 1318–1329. doi:10.1785/0220180372

Trevlopoulos, K., Guéguen, P., Helmstetter, A., and Cotton, F. (2020). Earthquake risk in reinforced concrete buildings during aftershock sequences based on period elongation and operational earthquake forecasting. *Structural Safety* 84, 101922. doi:10.1016/j.strusafe.2020.101922

Utsu, T. (1961). A statistical study of on the occurrence of aftershocks. *Geophysical Magazine* 30, 521–605.

Villiger, L., Gischig, V. S., Doetsch, J., Krietsch, H., Dutler, N. O., Jalali, M., et al. (2020). Influence of reservoir geology on seismic response during decameter-scale hydraulic stimulations in crystalline rock. *Solid Earth* 11 (2), 627–655. doi:10.5194/se-11-627-2020

Woessner, J., Hainzl, S., Marzocchi, W., Werner, M. J., Lombardi, A. M., Catalli, F., et al. (2011). A retrospective comparative forecast test on the 1992 Landers sequence. *J. Geophys. Res.* 116, B05305. doi:10.1029/2010JB007846

Yang, H. F., Wang, D., Guo, R. M., Xie, M., Zang, Y., Wang, Y., et al. (2022). Rapid report of the 8 january 2022 menyuan *Ms*6.9 earthquake, Qinghai, China. *Earthquake Research Advances* 2 (1), 100113–100114. doi:10.1016/j.eqrea.2022.100113

Zechar, J. D. (2010). "Evaluating earthquake predictions and earthquake forecasts: A guide for students and new researchers, *Community online resource for statistical seismicity analysis* 126. doi:10.5078/corssa-77337879

Zhang, C. J., Hou, Y. Y., Hu, B., Xu, H. H., and Wang, D. B. (2011). Analysis on the seismic activities and hazards of M7.1 earthquake, 2010 and M6.3 earthquake, 2011 in New Zealand. *Recent Developments in World Seismology* 1 (4), 44–51. doi:10.3969/j.issn.0235-4975.2011.04.010

Zorn, E., Kumar, A., Harbert, W., and Hammack, R. (2019). Geomechanical analysis of microseismicity in an organic shale: A West Virginia marcellus shale example. *Interpretation* 7 (1), T231–T239. doi:10.1190/int-2018-0072.1